Quantitative imaging of acoustic reflection and interference

2015 J. Phys.: Conf. Ser. 581 012007

(http://iopscience.iop.org/1742-6596/581/1/012007)

Quantitative imaging of acoustic reflection and interference

Robert Malkin[1], **Thomas Todd**[2] **and Daniel Robert**[1]

[1]School of Biological Sciences, University of Bristol, England, BS8 1TQ
[2]Faculty of Engineering, University of Bristol, England, BS8 1TR

E-mail: r.e.malkin@gmail.com

Abstract. This paper presents a method for time resolved quantitative imaging of acoustic waves. We present the theoretical background, the experimental method and the comparison between experimental and numerical reconstructions of acoustic reflection and interference. Laser Doppler vibrometry is used to detect the modulation of the propagation velocity of light, c, due to pressure-dependant changes in the refractive index of air. Variation in c is known to be proportional to variation in acoustic pressure and thus can be used to quantify sound pressure fluctuations. The method requires the laser beam to travel through the sound field, in effect integrating pressure along a transect line. We investigate the applicability of the method, in particular the effect of the geometry of the sound radiator on line integration. Both experimental and finite element reconstructions of the sound field are in good agreement, corroborating punctual pressure measurements from a precision microphone. Spatial limitations and accuracy of the method are presented and discussed.

1. Introduction

Quantified reconstruction of acoustic fields is commonly done using microphone arrays. These arrays tend to be expensive, bulky and uncertainty arises at higher frequencies where microphones can interfere with the sound field. Schlieren photography is a well-known method of visualising acoustic fields but lacks the ability of simple pressure field quantification [1]. The calculation of instantaneous sound pressure using light intensity measurements has been shown to be sensitive and accurate [2]. The use of laser Doppler vibrometry to measure acoustic fields has received prior attention [3]–[8], including tomographic 3D field reconstruction [9]. Previous research has shown that quantified sound field visualisation is possible but the implementation has been complex and results difficult to interpret. Here, we present a simple method (accessible to the non-specialist) of calculating the instantaneous pressure in air and show the importance of using an appropriate sound source for quantified field reconstruction.

2. Theory of refracto-vibrometry

The refractive index, n, of a medium is defined as;

$$n \equiv \frac{c_0}{v} \tag{1}$$

With c_0: velocity of light in a vacuum and v: the velocity of light in the medium. The refractive index of air is influenced by pressure, temperature, humidity and frequency (although the dispersive effect is relatively minor in standard conditions) [10]–[12]. In a simple adiabatic system a change in pressure results in a corresponding change in n. The resulting changes in propagation velocity, v, can be measured using a laser Doppler vibrometer (LDV) [4], [5], [13]. The technique of refracto-vibrometry has primarily been used for acoustic pressure visualisation in air and water [9], [13]–[16]. The principle of the measurement technique is described by Nakamura *et al* [17] and is illustrated in Figure 1.

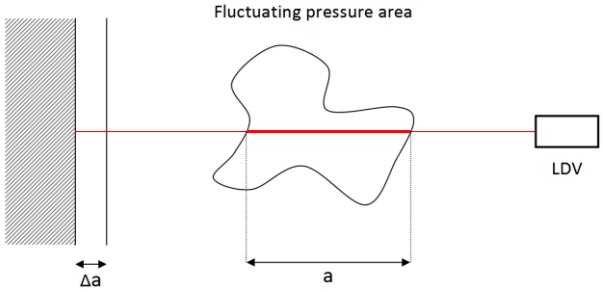

Figure 1. Using LDV, a rigid wall (shaded structure on the left) appears to be displaced by a distance of Δa . This is due to the modulation of the velocity of light propagation within the length *a* within the fluctuating pressure area**.**

Monochromatic laser light travelling through a region of sound pressure of length *a,* results in a corresponding variation in the magnitude of *n*. The laser light exits the region and, if reflected from a rigid wall, travels back through the region and back the LDV. This modulated path appears identical to a physical displacement of the reflective rigid wall, Δa.

$$n \cdot \Delta a = \Delta n \cdot a \tag{2}$$

Where the apparent displacement of the rigid wall, Δa, is given by integrating the LDV velocity (with respect to time) output signal. It has been shown that the pressure-refraction relation may be expressed in terms of temperature, pressure and relative humidity [18]. It is formalised by the expression:

$$n = 1 + \frac{7.86 \cdot 10^{-4} \cdot P}{273 + T} - (1.50 \cdot 10^{-11}) \cdot RH(T^2 + 160) \tag{3}$$

With P: pressure in kPa, T: temperature in °C and RH: relative humidity in %. At 1 atmosphere of pressure, 20°C temperature and a relative humidity of 50%, equation (3) gives *n* a value of 1.0002714. This relation between pressure and *n* allows us to relate the (observed) apparent displacement of the rigid wall to the pressure in the region of interest. Assuming an adiabatic process,

$$\frac{\Delta n}{\Delta P} = \beta = 2.68 \cdot 10^{-9}\ per\ Pa \tag{4}$$

Combining equations (2) and (4);

$$\Delta P = \frac{\Delta n}{2.68 \cdot 10^{-9}} = \frac{n}{a} \cdot \frac{\Delta a}{\beta} \tag{5}$$

The method of operation requires the laser to pass through the length of the region, *a*, meaning that the resulting velocity change is the integration of the average pressure distribution along the length of the path. As the laser travels from the LDV to the reflector and back, the resulting measured velocity from the LDV is an integration along the whole path length. The pressure field is likely to be variable along this length, therefore quantification of the field using equation (5) is complicated as the length *a* is unknown, as detailed by Olsson & Tatar in 2006 [7]. These authors noted that "any quantitative data obtained when measuring 3D sound fields using laser vibrometry must be viewed with some scepticism" due to the line integration problem when using a point source. In 2007, however, Olsson showed that the method could be used to measure the pressure magnitude correctly by using a correction factor [19]. While the results were accurate, Olsson's method did not lend itself to simple measurement of sound fields, requiring considerable technical expertise. Zipser *et al* took the approach of using a solid glass partition as a waveguide thereby constraining the region in which the sound was propagating [14]. This approach results in accurate quantification, yet precludes the use of free field conditions.

A rigorous treatment on the effect of pressure modulation on the optical laser path is detailed by, Torras-Rosell *et al* in [9].

3. Theoretical analysis of line integration of acoustic pressure

Here we use a 2D transient finite element analysis (FEA) (Comsol 4.3) model of acoustic pressure at 5, 10 & 20kHz for two acoustic radiators; a point source and a planar loudspeaker (with a width, *w*, of 150mm, equal to that of the speaker used in experiments), shown in Figure 2.

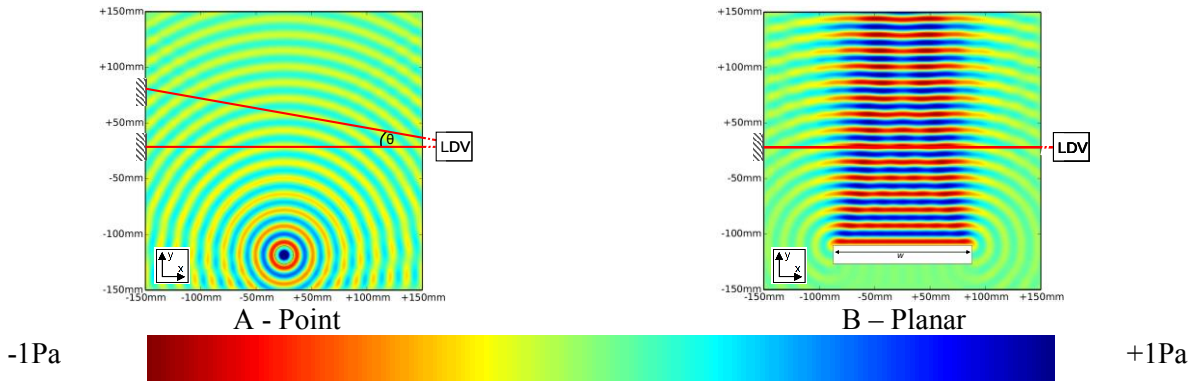

Figure 2. Simulated sound fields at 20kHz showing the position of the LDV, the rigid reflector (hatched area on Y-axis) and the scanning angle θ. A. Visualisation of acoustic field radiating from point source with 2 scan lines drawn. The laser beams from the LDV are shown with deviation angle θ, highlighting the alteration of the laser light path across the sound field. B. Visualisation of acoustic field radiating from a planar source.

In the experimental situation, the laser scanner (Polytec PSV-400) controls the position of the laser beam using rotating mirrors. This results in scan lines that are non-parallel, fanning out from the LDV with angle θ (shown in Figure 2A). The effect of the radiating geometry of the laser beam was investigated by Solodov et al [20]. For the present experimental work, the distance from the LDV to the reflecting wall (2m) was such that the maximum scanning angle was 2.6°. To investigate the effect of these non-parallel scan lines for the planar source case, the average pressure along a scan line (red line, Figure 2B) is compared to a point measurements along the y-axis for y>0mm at x=0mm. The results of this theoretical model-based analysis at 5, 10 and 20kHz are shown in Figure 3 for scanning angles up to 4° at one single phase of the sound pressure. This analysis reveals that for the outermost scan lines, the pressure value may be underestimated by as much as 15% for 20kHz. The error increases with frequency as the wavelength shortens and scan lines 'traverse' an increasing number of

wave fronts. This error can be reduced by: 1. increasing the distance between LDV and reflecting wall, 2. reducing the width of the planar loudspeaker w and 3. increasing the wavelength. These three optimisations can be used individually or in combination. For the FEA we assume the scan lines as to be parallel. It should be noted that for the non-parallel situation and higher frequencies, wavelengths can become sufficiently short as to cause considerable measurement error.

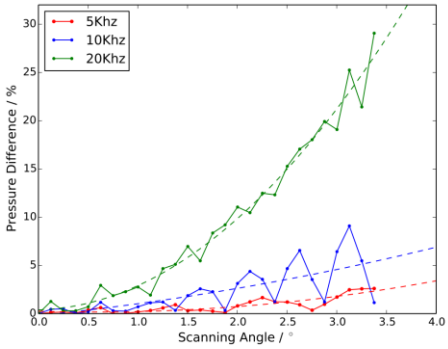

Figure 3. Experimental data of the effect of non-parallel scan lines on actual and line averaged pressure values taken at a single phase of sound pressure. Dashed lines show polynomial fit to data.

3.1. Instantaneous and cumulative pressure

The experimental measurements provide pressure estimates that are an average along the line of integration. The FEA models, however, allow us to probe the instantaneous pressure values along a line of integration, and study the phenomenon in greater detail. Simulating the line integration effect for a sound source of known geometry is useful to investigate the practicality of the LDV method for accurate measurements of pressure fields.

First, the instantaneous pressure value along a single scan line (as in Figure 2) was plotted as a function of the distance along that scan line (Figure 4A&C). Then, the cumulative pressure value is calculated along the same scan line (Figure 4B&D). The total cumulative pressure value, defined here as δ, is estimated as ≈-750Pa and ≈+7,000Pa for point and planar sources, respectively. δ is in effect equivalent to the instantaneous velocity signal from the LDV. We then define the coordinates along the scan line where the cumulative pressure equals 0.95δ (black dots in Figure 4). The 5% is used to reduce the number of data points (black dots), simplifying the analysis without compromising accuracy. Thresholds between 0.9δ and 0.99δ gave similar results, but data were visually less accessible when overlaid onto the pressure distribution.

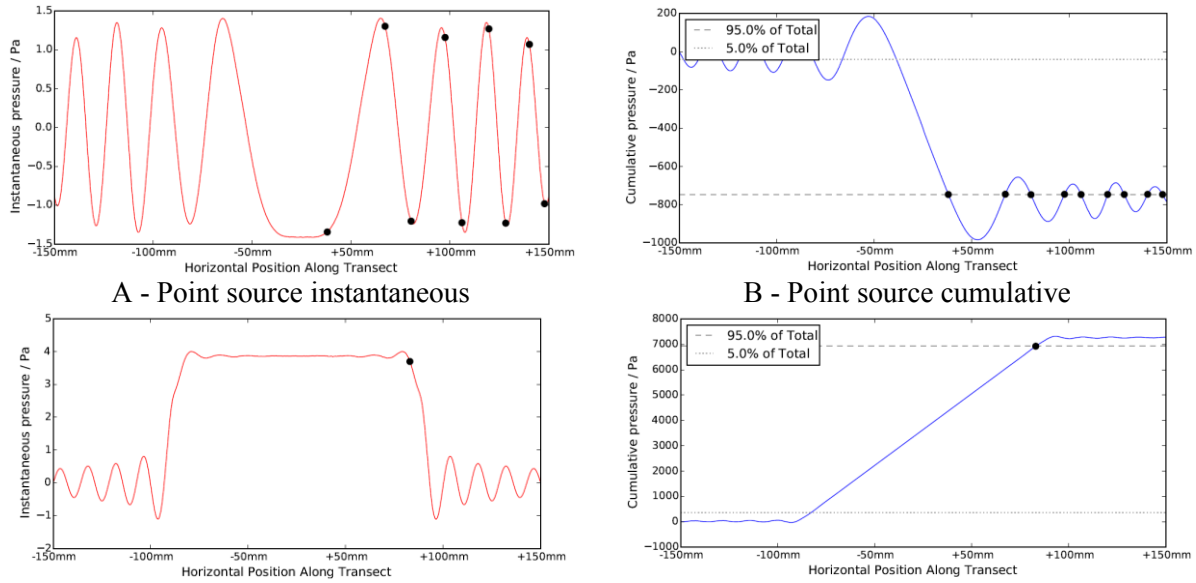

Figure 4. Modelled instantaneous (A-C) and cumulative (B-D) pressure values for a point (A-B) and planar (C-D) radiator, as shown in Figure 2. Black dots indicate locations of equal cumulative pressure, shown only for horizontal position x>0mm.

We then map these coordinates into the instantaneous pressure plots Figure 4A&C. This analytical procedure allows the measurement of the locations along the scan line that contributed to the observed average pressure. There are situations where multiple points reach the average cumulative pressure of 0.95δ. The physical interpretation of this is that the measured average cumulative pressure can be a contribution from several locations along the scan lines, thereby making the effective beam width, a, difficult to establish for a point source. This results in uncertainty about the quantitative interpretation of the LDV signal, and points to the importance of determining the width of the acoustic beam a.

3.2 Acoustic beam width, a

The points in the scanning area that show an instantaneous pressure value equal to 0.95δ were overlaid onto the pressure distribution plot (Figure 5). The sound field was probed using 220 parallel scan lines (corresponding to 15 scan lines per wavelength at 20kHz). This clearly highlights the regions within the scan area where instantaneous pressure contribute to the measured average. The magnitude of the acoustic field can also be computed for different phases; these data are shown in Supplementary Material 1.

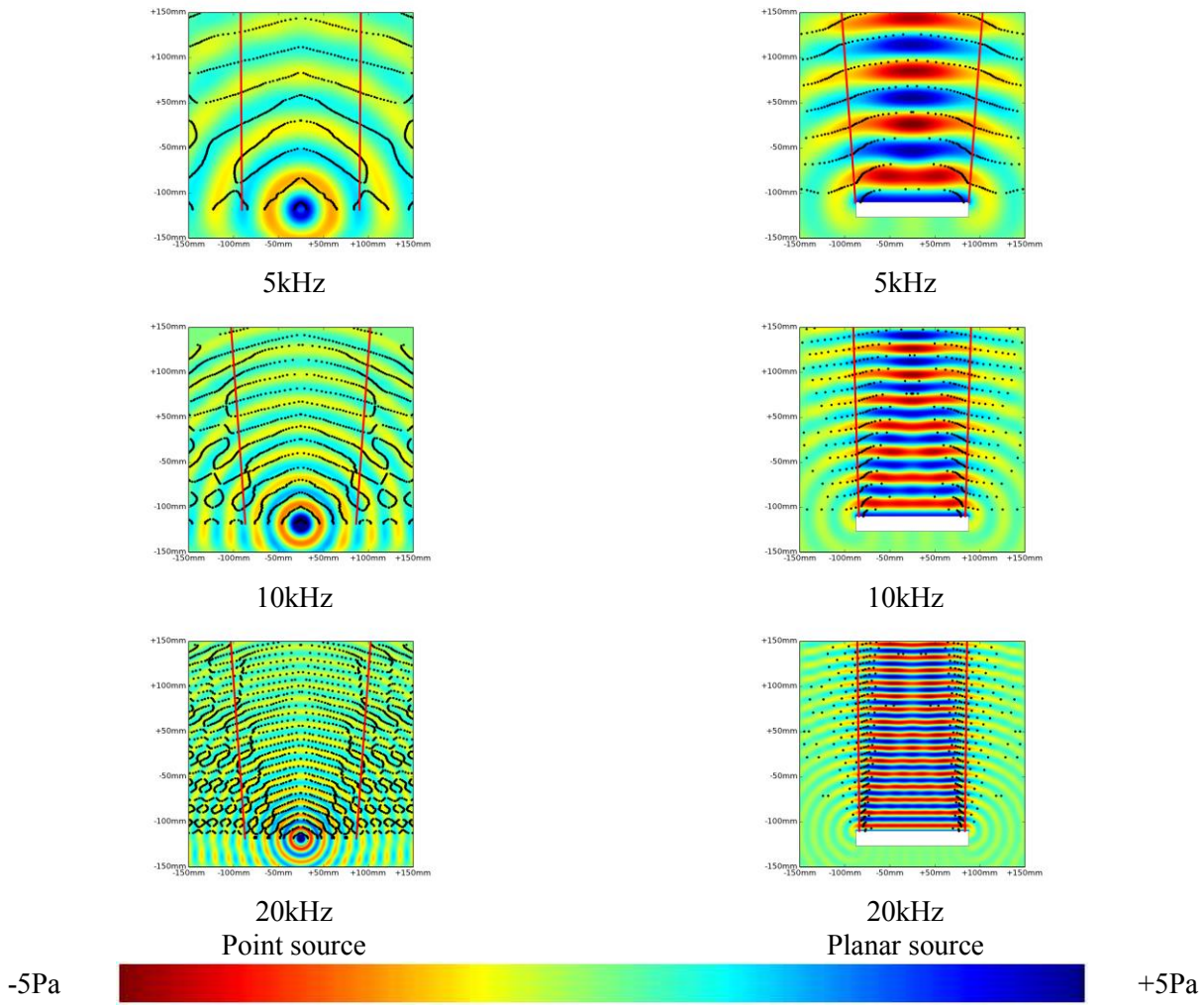

Figure 5. FEA models showing effective beam width for point and planar sources at 5, 10 and 20kHz. Black dots used to estimate beam width as shown in Figure 4. Solid red line shows linear fit to the black points. Red lines are used to calculate the angular divergence (taken as half the angle at the point where both lines meet).

The average width of the acoustic beam, a, was determined by plotting the black dots in a histogram (Figure 6), showing results for 20kHz (histograms for other phases and frequencies are in Supplementary Material 1). The 0.95δ distribution for the planar source yields two clear peaks, revealing the magnitude of beam width a. For the point source producing spherical waves, however, the 0.95δ distribution is also bimodal, yet no clear boundary emerges that permits the unambiguous determination of a.

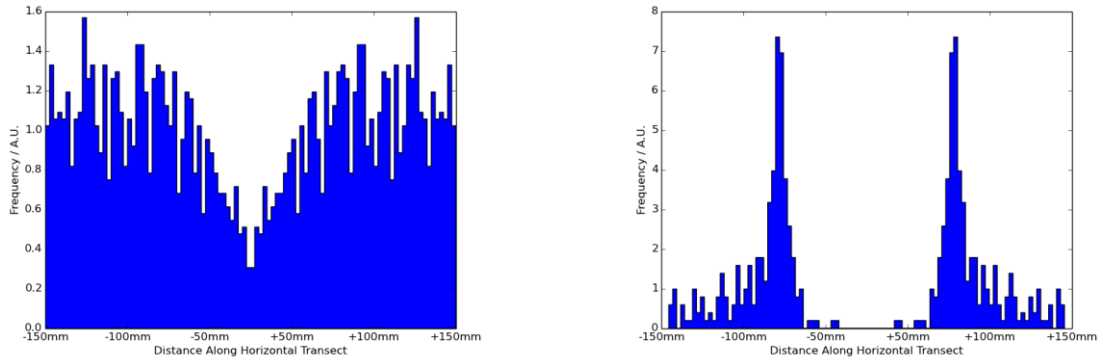

Point source Planar source

Figure 6. Histograms of black dot distributions shown in Figure 5 taken at the same point in time at 20kHz. The point and planar sources clearly differ whereby the latter exhibits two clear peaks with sharp boundaries, defining a.

3.3 Temporal stability and angular divergence of the acoustic beam

The analysis of the sound field at different phase angles allows for the measurement of the angular divergence (defined as half the angle made by the two linear regression lines in Figure 5) of the acoustic beam (Figure 7). The linear regression lines for the point source have very low R^2 values (around 0.002) due to the very large amount of scatter; they are shown here for direct comparison between point and planar sources.

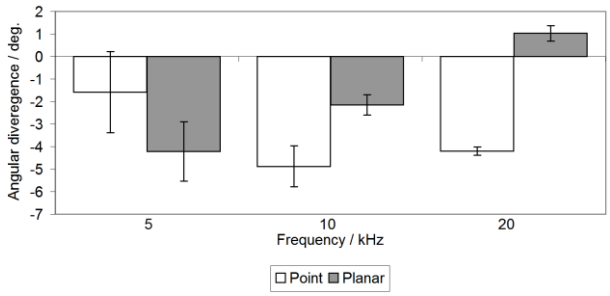

Figure 7 - Calculated angular beam divergence for 5, 10 and 20 kHz. Error bars are ±1 standard deviation, based on divergences measured at various phase angles along the pressure cycle.

The highly scattered black dots for the point source at all tested frequencies (Figure 5 and Figure 6) do not allow for simple estimation of a. For the planar source, the dual peak distribution allows for ready estimation of the beam width. This theoretical analysis provides evidence that a, and its variation calculated at different phase angle can be determined quantitatively using LDV refractometry only for a planar wave front (Figure 8). The analysis also shows the severe limitations encountered for an ideal single point source.

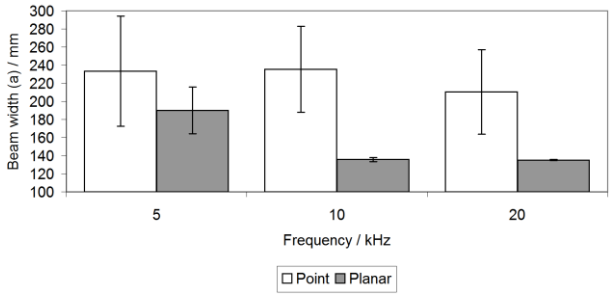

Figure 8. Width of the acoustic beam for different frequencies. Error bars are ± 1 standard deviation, based on measurements at various phases of the cycle.

4. Imaging of the acoustic field

4.1. Experimental procedure

Acoustic reflection and interference were investigated using laser Doppler refractometry, and employing the analytical rationale described above.

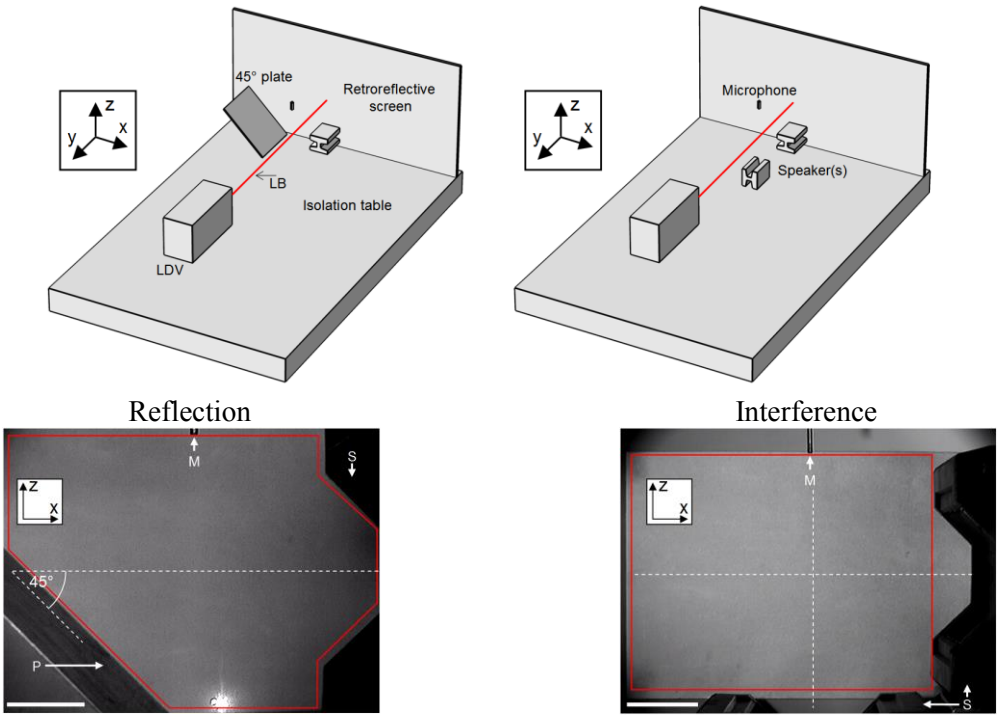

Figure 9. Experimental setup to visualise acoustic reflection and interference. Top panels: Diagrammatic representation of components and their relative positions in experimental setup (not to scale). Red line denotes the path of the laser beam. Bottom panels: Images from LDV showing the scanning area (outlined in red). Scale bars: 50mm. M: microphone, P: plate, S: loudspeaker, LB: laser beam.

The structure and propagation of acoustic waves were visualised for a wave packet of 5 cycles at 20kHz. Other experiments, using frequencies between 5-20kHz and other continuous tones showed similar results. Continuous tones however suffered from noisy signal from the numerous reflections within the acoustic booth used. The 5-cycles wave packet corresponds to 250µs signal duration at 20kHz, a time short enough to allow for repeat measurements (n=50) at each of the scan points, prior to the linear averaging of the velocity signal. The acoustic signal was generated by a waveform

generator (Agilent 33120A), and fed to the high frequency planar loudspeakers (AMT-1, ESS laboratories). The sound radiating Mylar membrane of the planar loudspeaker had a rectangular shape of 150mm length and 5mm width. Sampling frequency of the LDV was 512kHz and spatial resolution was set at 15 measuring points per wavelength in air. At 20kHz, this corresponds to ca. 9 points per centimetre. For all measurements, a calibrated precision reference microphone (Brüel & Kjær type 4138) was placed next to the observed pressure field, using a preamplifier (Brüel & Kjær, type 2633), and power supply (Brüel & Kjær, type 5935). The microphone signal is used to provide a calibrated reference in dB sound pressure level (SPL) (re. 20μPa).

One conceivable caveat of the method is that the acoustic energy from the loudspeakers could mechanically actuate the rigid wall used as the reflector. In effect, the laser signal does not distinguish between a fluctuation of the air refractive index along the line of integration and the sound-induced motion of the reflective wall. To investigate whether the recorded signals are affected by such mixing, a loudspeaker was positioned behind the reflective wall and vibrations (which in this case should be purely mechanical) on the reflective wall were measured. At the sound pressures and frequencies used here, the mechanical displacement velocity of the wall did not exceed background noise at all frequencies considered (5-20kHz). This control measurement prompts the conclusion that the reflective wall is indeed rigid during testing and does not contribute any velocity signal to the line of integration.

4.2. Imaging of the acoustic reflection

The reflection experiment reveals the time-resolved evolution of the wave packet as it encounters a reflective aluminium plate of 3mm thickness. Here, a single loudspeaker was positioned such that its acoustic axis was directed towards the aluminium plate at 45° angle of incidence (Figure 9). The temporal evolution of the pressure field was only measured in the space between the loudspeaker and the plate (Figure 10 & Animation 1). Pressure values were calculated from LDV displacement values for each scanning point using equation (5) (with a length of a as determined in 3.3).

For time, $0<t<3.9T$ (T: period at 20kHz), the wave packet is seen to propagate towards the aluminium plate. At t=3.9T the first sign of reflection and interference become apparent. The loudspeaker's inertia results in additional oscillations visible in the wake of the initial wave packet, detectable after t>1.3T, and absent in the FE model. At $t = 6.6T$ the wave packet is half reflected from the plate, giving rise to the interference pattern. At $t > 9.2T$ the wave packet has been fully reflected at an angle of 90°.

The experimental data is in good agreement with the finite element simulation, generating near to identical patterns of constructive and destructive interference (Figure 10). LDV and FE simulation pressure field coincide, lending strong support to the claim that the temporally accurate and spatially-resolved visualisation of the acoustic field is possible. There is, however, some disagreement between the measured and predicted pressure values (Figure 10, $t = 0.0T$) very close to the loudspeaker, where the FE model predicts higher pressures than the LDV. This discrepancy is likely due to two distinct effects. First, a small measurement error is introduced from the non-parallel scanning lines. Second, and more importantly, this region of the acoustic field is well within the loudspeaker's near-field, where the structure of sound pressure is notoriously complicated. In fact, little experimental information is available on sound field geometry in the near-field, an outstanding question amenable to the approach presented here.

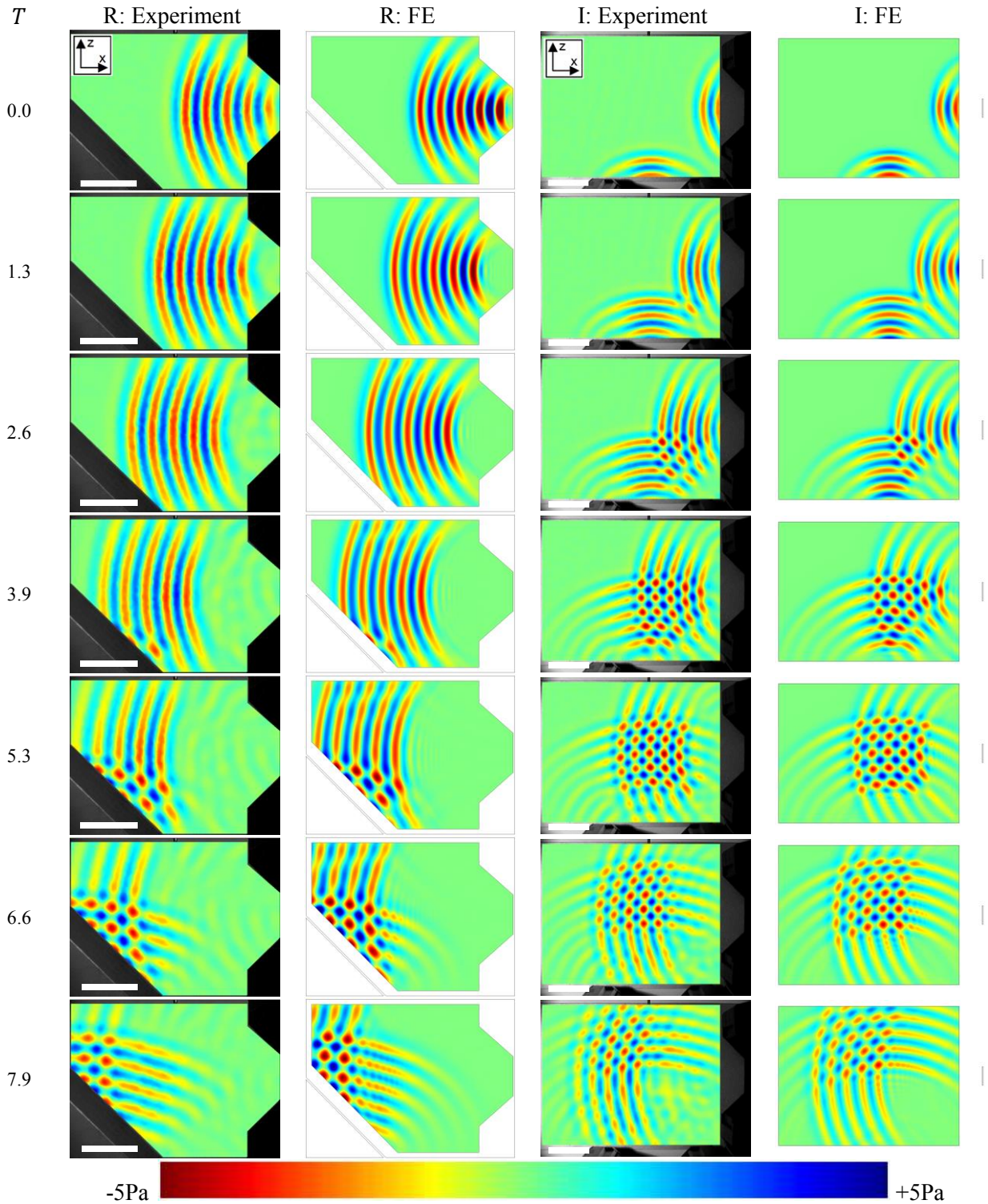

Figure 10a. Experimental and FE representations of pressure field with increasing time steps. Scale bar: 5cm. *T*: period (*T*=50μs), R: reflection, I: interference.

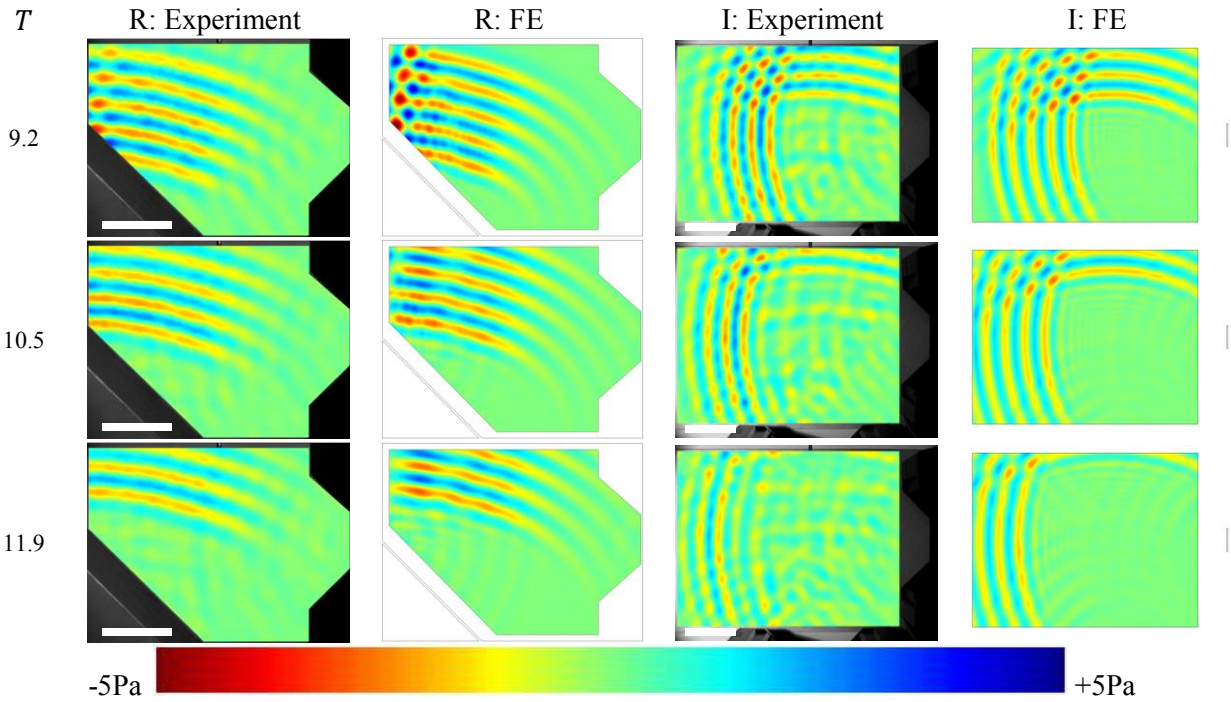

Figure 10b. Experimental and FE representations of pressure field with increasing time steps. Scale bar: 5cm. T: period (T=50μs), R: reflection, I: interference.

4.3. Imaging of the acoustic interference

Acoustic interference was generated using two loudspeakers, oriented at 90° to each. LDV refractometry was then used to image the temporal evolution of the sound field as the two synchronously radiated and identical wave packets interfered (Figure 10 & Animation 2). Interference patterns begin to appear at $t = 1.3T$ and develop fully by $t = 5.3T$. For $t > 5.3T$, the wave packets continue to propagate with only some regions undergoing interference. The structure of the pressure field reveals that some regions are free of interference, where the wave packets propagate independently from each other. Interestingly, the mesh-like region of interference is observed to propagate exactly along a 45° diagonal. For $t > 7.9T$, some afterwaves are observed by the LDV, again resulting from the loudspeakers mechanical inertia. As with the reflection experiment, there is good spatial and temporal agreement between FE simulation and LDV (Figure 10).

4.4. FEA simulation of reflection and interference

Reflection and interference were simulated using a time-dependent acoustic pressure model. A model 2D space of 300mm × 300mm with 15 quadratic triangular elements per wavelength was used. A mesh convergence study was carried out, showing that 6 elements/wavelength would be sufficient to represent the sound field. Yet, at low computational cost, 15 elements were used to match the experimental spatial resolution. The models included an acoustic source boundary to simulate the loudspeaker(s), a sound radiation boundary to simulate the waves propagating out of the model space, and a sound hard boundary to simulate a reflecting surface. The number of elements used was 45k for reflection and 48k for the interference experiments. Results of both simulations are shown in Figure 10. As with most loudspeakers, producing a finite wave packet is difficult to achieve due to the mechanical inertia of the sound radiating elements, therefore some differences in the experimental and FEA results are expected for the trailing edge of the wave packet. As the FEA stimulus is ideal, direct FEA-LDV comparison could be used to investigate the quality of sound radiators in unprecedented temporal and spatial detail.

4.5 Critical evaluation of the method

To verify the quantitative validity of the method, the acoustic pressure measured by LDV was compared to that of the reference microphone. LDV time-resolved signal was taken from a measurement point 1mm away from the microphone (Figure 11). This comparison corroborates previous reports that laser interferometry can be used to infer pressure from refractive index modulation [9] [21]. There is good agreement between microphone and calculated LDV pressure, both in magnitude and phase (Figure 11). Some differences exist between the two signals that are not fully understood. A key difference resides in the fact that the precision microphone detects pressure changes in all three spatial directions, whereas the LDV measurement reports pressure changes along the direction of the laser path, the integration line. In addition, the microphone is detecting sound pressure over a region of air, of unknown volume and geometry. It may therefore be possible that LDV integration done at 1 mm distance does not reflect in detail the pressure integrated by the pressure microphone. To date, information on the actual acoustic sampling of microphones does not provide the spatial details necessary to resolve this issue. The technique presented, applied with an increased scanning resolution, can however be useful to perform such detailed analysis.

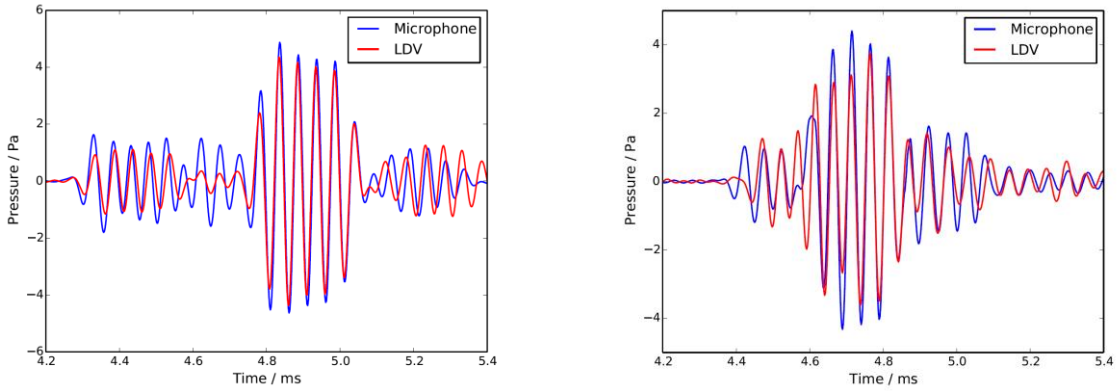

Figure 11 – Comparison of sound pressure for reference microphone and LDV pressure measurements. LDV point taken 1mm from microphone tip.

5. Discussion

We have shown that a quantitative spatial and temporal reconstruction of acoustic waves can be achieved by way of laser Doppler vibrometry and simple transformation of the velocity signal. This study also shows that the geometry of the sound source is an important factor to consider regarding the accuracy of line integration and therefore for the reconstruction of acoustic fields. The measurement error introduced by non-parallel scanning lines can be reduced by a conjunction of three methodological adjustments; the use of a planar loudspeaker with narrow beam width, a sufficiently large laser-reflector distance and suitably large wavelengths. The use of a telecentric lens in the LDV would contribute to the optimisation and flexibility of the technique.

The FEA data (Figure 5) and analysis (Figure 8) together suggest that the effective acoustic beam width of the point source is unstable for the frequencies considered. From Figure 4A it is apparent that multiple points along the integration line contribute to the average signal. The present analysis shows that the quantification of sound pressure radiating from a point source is ambiguous. While the sound field can be visualised, a quantitative approach appears not to be practical at the moment. For the planar source, however, a calculated estimate of the beam width is possible. Whilst the spatial scatter of the beam width, a, for the point source is very large irrespective of frequency (Figure 8), the planar source yields values of a with a clear structure for frequencies >5kHz, revealing a high temporal stability for 20kHz.

Surface reflection and interference hae been accurately reconstructed in terms of spatial organisation, magnitude and phase. FEA corroborates the experimental field visualisation, providing a good match to LDV (Figure 10). The LDV refractometry method also accurately reports on sound pressure level, as confirmed by comparison to a reference precision microphone (Figure 11).

The phenomenological explanation for the line integration phenomenon and the observable pressure field highlights the importance of the geometry and orientation of the integration path. Knowledge of a is required for a correct calculation of the average sound pressure within the observable pressure field, as shown by equation (5). The exact shape of this region is dependent upon the geometry of the acoustic radiator, the distance between the laser beam and the sound radiator, the acoustic interactions with nearby structures, and sound frequency. One consequence is that in sound fields comprising complicated reflective structures, the effective value of a may vary with orientation, setup geometry and sound frequency.

6. Conclusions

The visualisation of sound fields is rarely used as a diagnostic or analytical tool in acoustic research, industrial noise analysis or product development. Refracto-vibrometry is shown here to be a rapid, accurate method that can lend itself to research and industrial applications. The present analysis shows that by carefully considering the geometry of the sound radiator, it is possible to produce accurate sound field imaging. The method presented here does not require extensive calculations and unwarranted assumptions, and therefore could find practical. While some limitations still exist, scanning refracto-vibrometry holds the promise of improving the non-contact, clutter-free quantitative evaluation of acoustic fields.

Acknowledgments

This research is part of a research programme on the mechanics of auditory systems funded by the BBSRC. DR acknowledges support from the Royal Society of London.

References

[1] Chinnery P A 1997 The schlieren image of wo-dimensional ultrasonic fields and cavity resonances *The Journal of the Acoustical Society of America* **101** 250–6

[2] Pitts T A and Greenleaf J F 2000 Three-dimensional optical measurement of instantaneous pressure. *The Journal of the Acoustical Society of America* **108** 2873–83

[3] Nakamura K 2001 Sound field measurement through the acousto-optic effect of air by using laser Doppler velocimeter *4th Pacific Rim Conference on Lasers and Electro-Optics* vol 1 (Chiba-Japan: IEEE) pp 154–5

[4] Zipser L, Franke H, Olsson E, Molin N E and Sjödahl M 2003 Reconstructing two-dimensional acoustic object fields by use of digital phase conjugation of scanning laser

[5] Vuye C, Vanlanduit S and Guillaume P 2009 Accurate estimation of normal incidence absorption coefficients with confidence intervals using a scanning laser Doppler vibrometer *Optics and Lasers in Engineering* **47** 644–50

[6] Jia X, Quentin G and Lassoued M 1993 Optical heterodyne detection of pulsed ultrasonic pressures. *IEEE transactions on ultrasonics, ferroelectrics, and frequency control* **40** 67–9

[7] Olsson E and Tatar K 2006 Sound field determination and projection effects using laser vibrometry *Measurement Science and Technology* **17** 2843–51

[8] Zipser L and Franke H 2007 Refracto-Vibrometry for Visualizing Ultrasound in Gases, Fluids and Condensed Matter *2007 IEEE Ultrasonics Symposium Proceedings* (IEEE) pp 395–8

[9] Torras-Rosell A, Barrera-Figueroa S and Jacobsen F 2012 Sound field reconstruction using acousto-optic tomography. *The Journal of the Acoustical Society of America* **131** 3786–93

[10] Wimberger-Friedl R 1995 The assessment of orientation, stress and density distributions in injection-molded amorphous polymers by optical techniques *Progress in Polymer Science* **20** 369–401

[11] Waxler R M and E W C 1965 Effect of Hydrostatic Pressure on the Refractive Indices of Some Solids *Journal of Research of the National Bureau of Standards -A* **69A** 325–33
[12] Edlén B 1966 The Refractive Index of Air *Metrologia* **2** 71–80
[13] Oikawa Y 2005 Sound Field Measurements Based on Reconstruction from Laser Projections *IEEE International Conference on Acoustics, Speech, and Signal Processing* vol 4 (Philadelphia-USA: IEEE) pp 661–4
[14] Zipser L, Seelig H-D and Franke H 2009 Refracto-vibrometry for visualizing ultrasound in small-sized channels, cavities and objects *International Ultrasonics Symposium* (Rome-Italy) pp 2588–91
[15] Olsson E 2009 Three-dimensional selective imaging of sound sources *Optical Engineering* **48** 035801
[16] Wang Y, Theobald P, Tyrer J and Lepper P 2004 The application of scanning vibrometer in mapping ultrasound fields *Journal of Physics: Conference Series* **1** 167–73
[17] Nakamura K, Hirayama M and Ueha S 2002 Measurements of air-borne ultrasound by detecting the modulation in optical refractive index of air *IEEE Ultrasonics Symposium* (Munich-Germany) pp 609–12
[18] Dittmar A and Behrendt R 2008 Measuring the 3D propagation of sound waves using scanning laser vibrometry *Berlin Beamforming Conference* (Berlin)
[19] Olsson E 2007 Selective imaging of sound sources in air using phase-calibrated multiwavelength digital holographic reconstructions *Optical Engineering* **46** 075801
[20] Solodov I, Döring D and Busse G 2008 Air-coupled laser vibrometry: analysis and applications *Applied Optics* **48** 33–7
[21] Balek R and Slegrova Z 2002 A Comparison of Acoustic Field Measurement by a Microphone and by an Optical Interferometric Probe *Acta Polytechnica* **42** 13–7

Supplementary Material 1

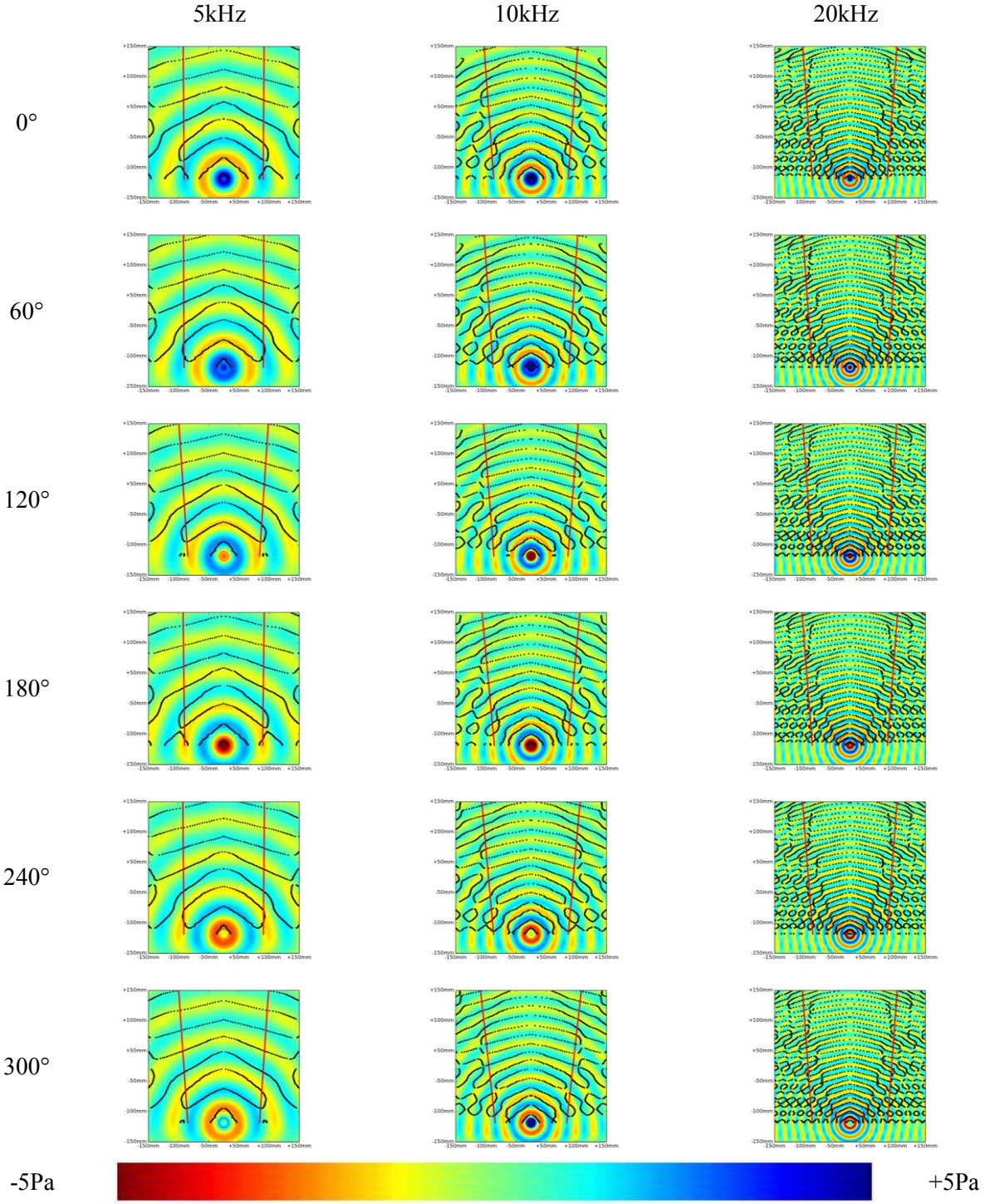

Figure S1 - Point source temporal stability.

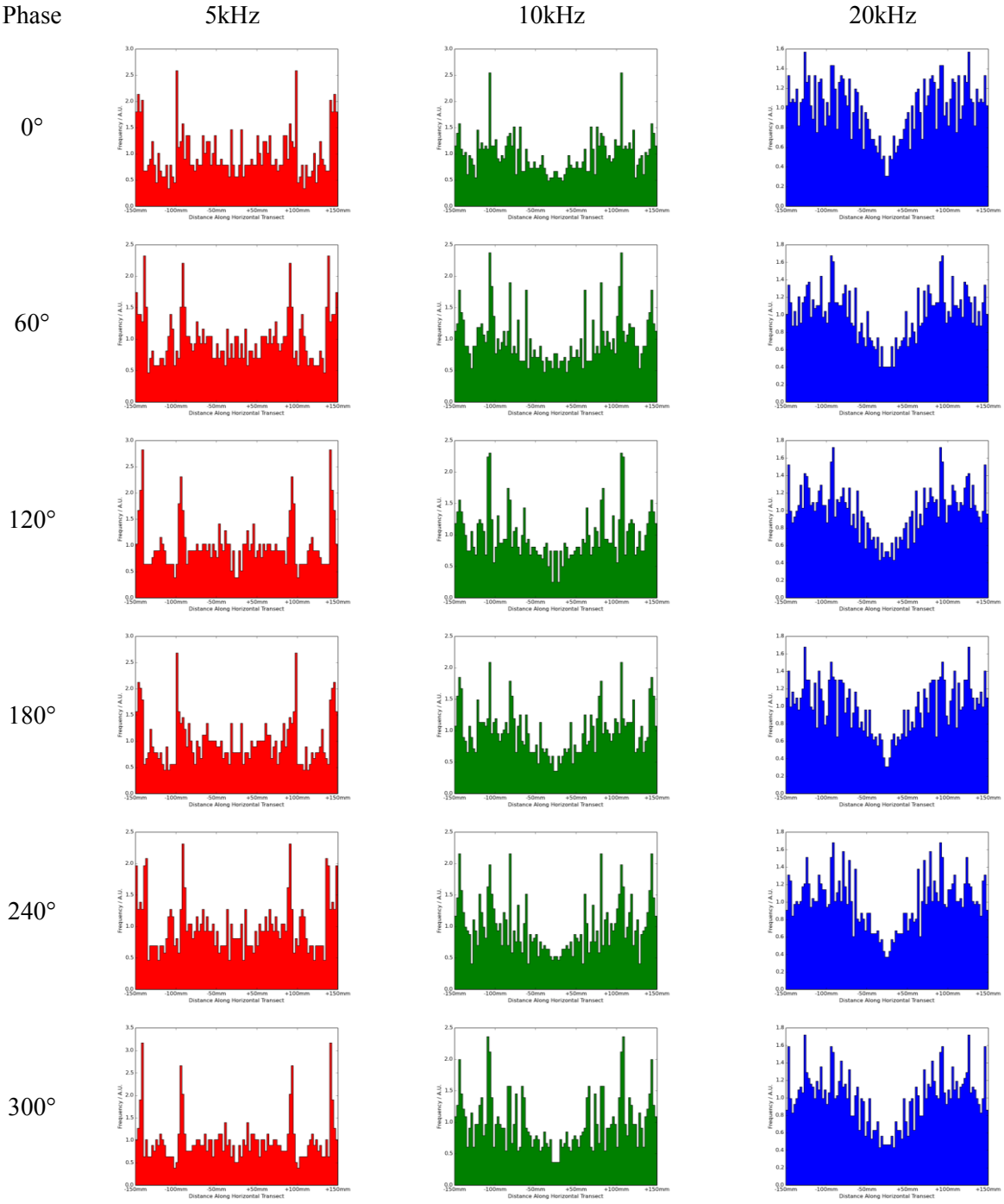

Figure S2 - Point source histograms.

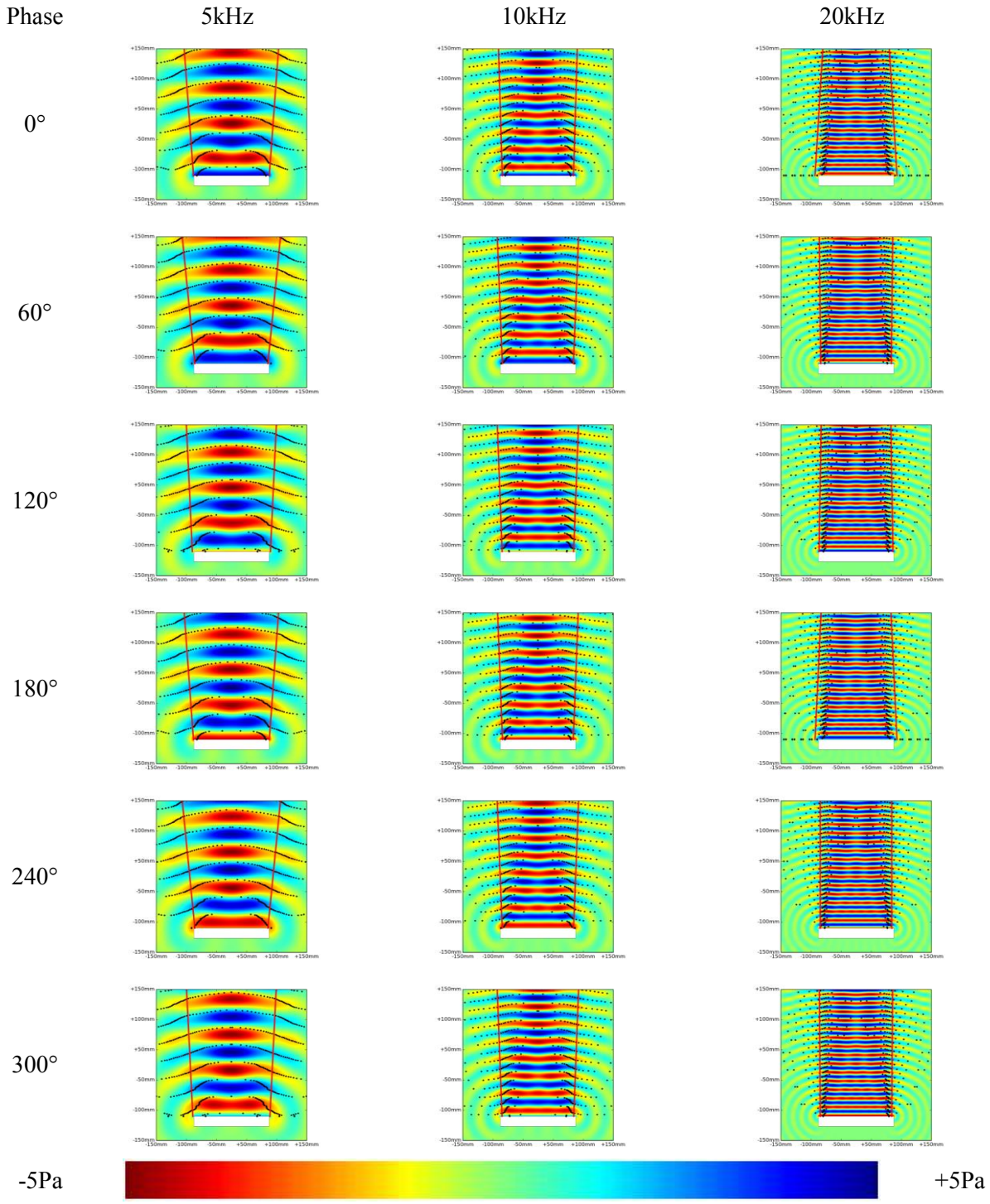

Figure S3- Planar source temporal stability.

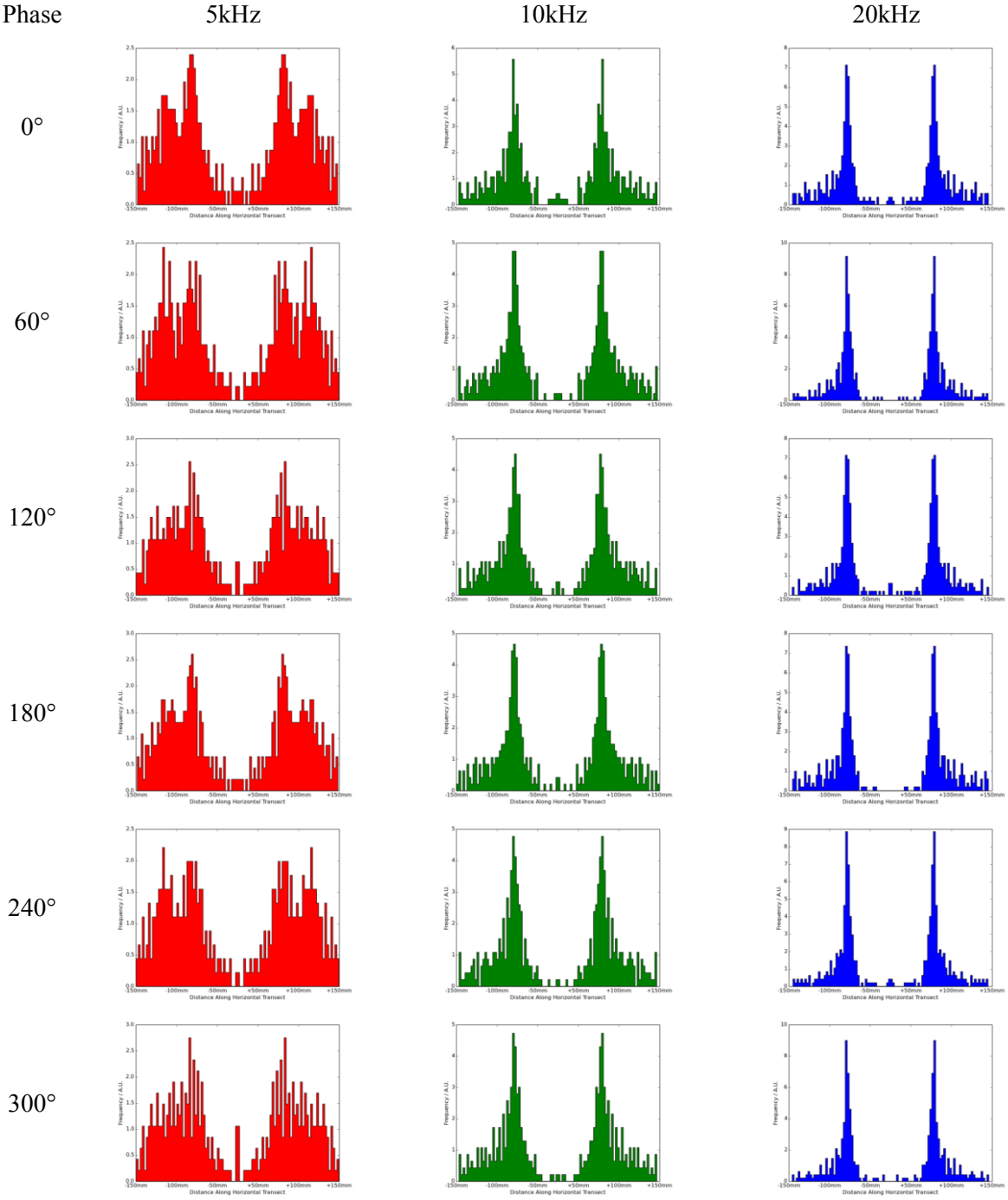

Figure S4 - Planar source histograms.